Editorial Manager(tm) for Journal of Computational Physics
Manuscript Draft

Manuscript Number: JCOMP-D-08-00001

Title: A Monolithic FEM Approach for Non-Isothermal Incompressible Viscous Flows

Article Type: Regular Article

Keywords: Monolithic FEM; Non-Isothermal; Incompressible viscous flow; Multigrid

Corresponding Author: Mr. Hogenrich Damanik,

Corresponding Author's Institution: TU Dortmund

First Author: Hogenrich Damanik

Order of Authors: Hogenrich Damanik; Jaroslav Hron, Dr.; Abderrahim Ouazzi, Dr.; Stefan Turek, Prof., Dr.

A Monolithic FEM Approach for Non-isothermal Incompressible Viscous Flows ⋆

H. Damanik [a,*], J. Hron [b], A. Ouazzi [a], S. Turek [a]

[a] *Institute of Applied Mathematics, Technical University of Dortmund, Germany*

[b] *Institute of Mathematics, Charles University, Czech Republic*

Abstract

We present special numerical simulation techniques for non-isothermal incompressible viscous fluids. The flow which is governed by the Boussinesq approximation and the Navier-Stokes equations is solved in a fully coupled monolithic way. For time discretization, we apply the fully implicit Crank-Nicolson scheme of 2nd order accuracy. We utilize the high order Q_2P_1 finite element pair for discretization in space to gain high accuracy with local grid refinement. The resulting nonlinear discrete systems are solved via a quasi-Newton method with a divided difference approach to handle the Jacobian matrices. In each nonlinear step, the discrete linear subproblems are solved by means of a special multigrid method with local multilevel pressure Schur complement smoothers. For validation of the presented methodology, we perform the MIT benchmark 2001 [3, 4] of natural convection flow in enclosures to compare our results with respect to accuracy and efficiency. Additionally, we simulate problems with temperature and shear dependent viscosity and discuss the effect of an additional dissipation term inside the energy equation.

Key words: Monolithic FEM, Non-isothermal, Incompressible viscous flow, Multigrid

⋆ This research was supported by the Graduate School of Production Engineering and Logistics and by the German Research Foundation (DFG) through the collaborative research center SFB/TR TRR 30 and through the grants TU 102/11-3 (FOR493) and TU 102/21-1

* Corresponding author.

Email addresses: hdamanik@math.uni-dortmund.de (H. Damanik), hron@karlin.mff.cuni.cz (J. Hron), ouazzi@math.uni-dortmund.de (A. Ouazzi), ture@featflow.de (S. Turek).

1 Introduction

Non-isothermal flow is very important in many applications since it is the basic of many complex flow problems with viscoelastic and multi-phase fluids. Air flow inside a combustion engine or polymer flow in an injection molding or fluid flow in a heat exchanger are few examples of viscous fluids where temperature is an important unknown. It becomes even more important when the fluid viscosity is temperature dependent. In this case, the temperature will indirectly give impact onto the velocity field through the viscosity, as we shall see later in the section 4. Since a reliable accuracy of the numerical solution is one of the main issues for such simulations, we utilize the LBB-stable conforming finite element pair Q_2P_1 which is known to be one of the "best" finite element pairs for incompressible flow and we solve for all physical quantities in a fully coupled monolithic way. Additionally, we apply local grid refinement techniques to reduce the total number of degrees of freedom while maintaining the numerical results to its best accuracy which is achieved via hanging nodes together with a hierarchical multigrid solver for handling the linear part.

The underlying flow model is governed by the Navier-Stokes equations which arise from the classical equations of continuity

$$\nabla \cdot \mathbf{u} = 0 \tag{1}$$

and the equations of motion with a body force term which is written as Boussinesq approximation

$$\rho \frac{\partial \mathbf{u}}{\partial t} + \rho(\nabla \mathbf{u})\mathbf{u} = \nabla \cdot \mathbf{T} + \rho(1 - \gamma\Theta)\mathbf{j} \tag{2}$$

where $\mathbf{T} = -pI + 2\eta\mathbf{D}$ describes the constitutive material law. The Navier-Stokes equations are coupled with an energy equation to include the effect of temperature

$$\frac{\partial \Theta}{\partial t} + \mathbf{u} \cdot \nabla\Theta = \frac{1}{\sqrt{Ra\ Pr}}\ \nabla^2\Theta \tag{3}$$

where $\mathbf{u}, \rho, \gamma, \mathbf{j}, p, \eta, \mathbf{D}, Pr, Ra, \Theta$ are the velocity, density, thermal expansion, gravity vector, pressure, viscosity, symmetric part of gradient velocity, Prandtl number, Rayleigh number and temperature (see [3, 4] for details).

In the numerical section we consider natural convection flow in enclosures from the MIT benchmark 2001 [3] to analyze the accuracy and efficiency of our non-isothermal code. This problem is well suited from the numerical point a view due to its simple geometry while at the same time complex phenomena in space and time arise. Moreover, this benchmark provides a large set of data for different approaches and methods to compare.

In the following, we discretize the flow problem in two dimensions by applying the Q_2P_1 finite element pair in a standard FEM approach. We solve the resulting discrete problems in a fully coupled monolithic way for $(\mathbf{u}, p, \Theta)$ utilizing multigrid with special smoothers for handling the linear sub-problems such that we maintain the high efficiency and robustness of classical linear FEM approaches (see [16]).

2 Spatial and Time Discretization

After discretizing the system (1) - (3) in time by the Crank-Nicolson scheme, we discretize in space by the finite element method using the Q_2P_1 element pair in two dimension. By Q_2P_1 we mean the standard 2D biquadratic space with 9 local degrees of freedom for each velocity/temperature component and 3 degrees of freedom for a piecewise linear discontinuous pressure approximation in each element. In 2D, there are in total 30 degrees of freedoms in each element consisting of velocity, temperature and pressure variables. In order to reduce the global degrees of freedom, we apply local grid refinement techniques by using hanging nodes in a proper way where the values of hanging nodes must satisfy the continuity constraint of the neighboring nodes so that the finite element function remains globally continuous and hence conforming.

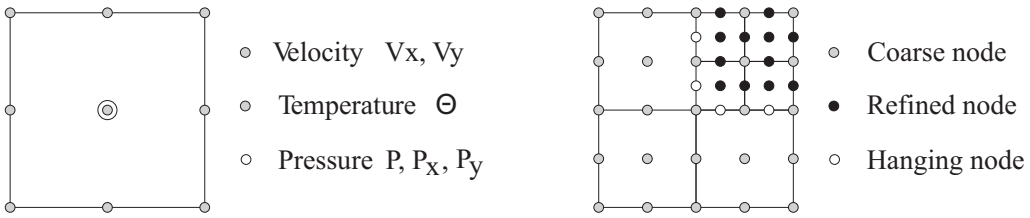

Fig. 1. *Left: Local degrees of freedom for Q_2P_1. Right: Locally refined element*

2.1 The conforming Stokes element Q_2P_1

As usual we define the finite dimensional spaces W_h for temperature, V_h for velocity and L_h for the pressure approximations as

$$W_h := \left\{ w_h \in H_0^1(\Omega_h) | \quad w_{h|T} \in Q_2(T) \; \forall T \in T_h, \quad w_h = 0 \text{ on } \partial\Omega_h \right\}, \tag{4}$$

$$V_h := W_h \times W_h, \quad \text{and} \tag{5}$$

$$L_h := \left\{ l_h \in L^2(\Omega_h) | \quad l_{h|T} \in P_1(T) \;\; \forall T \in T_h \right\}, \tag{6}$$

and consider for each $T \in T_h$ the standard bilinear transformation $\psi_T : \hat{T} \to T$ from $\hat{T}$ to the unit square T. Then, $Q_2(T)$ is defined as

$$Q_2(T) := \left\{ q \circ \psi_T^{-1} | q \in \text{span} < 1, x, y, xy, x^2, y^2, x^2y, y^2x, x^2y^2 > \right\} \quad (7)$$

with nine local degrees of freedom located at the vertices, at the midpoints of the edges and in the center of the quadrilateral T. The space $P_1(T)$ consists of linear functions defined by

$$P_1(T) = \left\{ q \circ \psi_T^{-1} : q \in \text{span} < 1, x, y > \right\} \quad (8)$$

with the function values and both partial derivatives located in the center of each quadrilateral T, leading to three local degrees of freedom which gives a discontinuous pressure. The inf-sup condition is satisfied (see [2]); however, the combination of the bilinear transformation ψ with a linear function on the reference square would imply that the basis on the reference square does not contain the full bilinear basis. So, the method can be only first order accurate on general meshes (see [1, 2])

$$\|p - p_h\|_0 = O(h). \quad (9)$$

The standard remedy is to consider a local coordinate system (ξ, η) obtained by joining the midpoints of the opposing faces of T (see [1, 10, 14]). Then, we set on each element T

$$P_1(T) := \text{span} < 1, \xi, \eta > . \quad (10)$$

For this case, the inf-sup condition is also satisfied and the second order approximation is recovered for the pressure as well as for the velocity gradient (see [2, 7])

$$\|p - p_h\|_0 = O(h^2) \quad \text{and} \quad \|\nabla u - \nabla u_h)\|_0 = O(h^2). \quad (11)$$

For a smooth solution, the approximation error for the velocity in the L_2-norm is of order $O(h^3)$ which can be easily demonstrated for prescribed polynomials or for smooth data on appropriate domains.

2.2 Implicit Time Integrator

We need to solve for velocity, temperature, and pressure at the current time step, $n+1$, using known values from the previous time step, n. A fully implicit method is utilized instead of an explicit time integrator because of the severe stability problems inherent in the explicit approach for incompressible flow

problems (see [15]). The Navier-Stokes equations are discretized in time as follows

$$\frac{\mathbf{u}^{n+1}-\mathbf{u}^{n}}{\Delta t}+$$
$$\theta\left[(\nabla\mathbf{u}^{n+1})\mathbf{u}^{n+1}-(1-\gamma\Theta^{n+1})\mathbf{j}-\frac{1}{\rho}(-\nabla p^{n+1}+2\nabla\cdot\eta\mathbf{D}(\mathbf{u}^{n+1}))\right] \tag{12}$$
$$+(1-\theta)\left[(\nabla\mathbf{u}^{n})+\mathbf{u}^{n}-(1-\gamma\Theta^{n})\mathbf{j}-\frac{1}{\rho}(-\nabla p^{n}+2\nabla\cdot\eta\mathbf{D}(\mathbf{u}^{n}))\right]=0$$

where $\mathbf{u}^n \sim \mathbf{u}(t_n)$. The energy equation is discretized in the same way so that

$$\frac{\Theta^{n+1}-\Theta^{n}}{\Delta t}+\theta\left[\mathbf{u}^{n+1}\cdot\nabla\Theta^{n+1}-\frac{1}{\sqrt{Ra\ Pr}}\ \Delta\Theta^{n+1}\right]$$
$$+(1-\theta)\left[\mathbf{u}^{n}\cdot\nabla\Theta^{n}-\frac{1}{\sqrt{Ra\ Pr}}\ \Delta\Theta^{n}\right]=0. \tag{13}$$

By choosing $\theta=\frac{1}{2}$ we obtain the fully implicit Crank-Nicolson method with second order accuracy. Then, by rearranging these equations into algebraic systems, we end up with the following nonlinear system of equations in each time step

$$\begin{pmatrix} S_u(\mathbf{u}^{n+1}) & 0 & j_1M & B_u \\ 0 & S_v(\mathbf{u}^{n+1}) & j_2M & B_v \\ 0 & 0 & S_\Theta(\mathbf{u}^{n+1}) & 0 \\ B_u^T & B_v^T & 0 & 0 \end{pmatrix}\begin{pmatrix} u^{n+1} \\ v^{n+1} \\ \Theta^{n+1} \\ p^{n+1} \end{pmatrix}=\begin{pmatrix} f_u(n+1,\ n) \\ f_v(n+1,\ n) \\ g(n+1,\ n) \\ 0 \end{pmatrix} \tag{14}$$

where S describes the reactive, diffusive, and convective terms from the governing equations above. Here, $\mathbf{u}=(u,v)$ consists of the component u and v.

3 Iterative Solvers

We apply the standard finite element method with the Q_2P_1 element pair as described above which leads to the nonlinear system of equation as in (14). This nonlinear system is then solved by a Newton iteration which has a well known quadratic convergence if the initial solution is chosen close enough to the exact solution. Turek et al. [13] have shown the excellent convergence rates of Newton iteration in comparison with fixed point methods for non-isothermal flow. The basic idea of the Newton iteration is to find a root of a function, $\mathbf{R}(\mathbf{X})=\ \mathbf{0}$, using the available known function value and its first derivative,

$$\mathbf{X}^{l+1}=\mathbf{X}^{l}+\omega^{l}\mathbf{J}^{-1}\mathbf{R}(\mathbf{X}^{l}) \tag{15}$$

with $\mathbf{X} = (\mathbf{u}_h, \Theta_h, p_h)$ in our setting and $\mathbf{J} = \left[\frac{\partial \mathbf{R}(\mathbf{X}^l)}{\partial \mathbf{X}}\right]$ is the Jacobian matrix. Here, $\mathbf{R} = \left(\text{def}_u^l \ \text{def}_v^l \ \text{def}_\Theta^l \ \text{def}_p^l\right)^T$ is the residual coming from the discrete problem of the system (14) and ω^l is some damping parameter which has to be determined such that certain error measures decrease (see [9, 14]). In the next step we will discuss how to deal with the Jacobian before we discuss how to solve the linear sub-problems in each nonlinear step. In our approach, we approximate the first derivative (the Jacobian) using divided differences

$$\left[\frac{\partial \mathbf{R}(\mathbf{X}^l)}{\partial \mathbf{X}}\right]_{ij} \approx \frac{\mathbf{R}_i(\mathbf{X}^l + \epsilon e_j) - \mathbf{R}_i(\mathbf{X}^l - \epsilon e_j)}{2\epsilon} \tag{16}$$

where $e_j = \delta_{ij}$ is the standard Kronecker symbol. Another possibility is to calculate the Frechét-derivative at the continuous level, which however can be very complicated for complex nonlinear flow models (see [13, 14]).

For small systems (i.e. less than 20.000 unknowns) a direct linear solver like UMFPACK is often preferable. But for large systems, its memory requirements are far too high. We choose as an alternative to use a multigrid method which is today one of the fastest iterative linear solvers for CFD problems (see [18]). Inside multigrid, restriction is applied to the residual after smoothing on all mesh levels and a direct linear solver is utilized to obtain the coarsest grid solution. Prolongation is then applied which is followed by post-smoothing to give a better approximation. These steps continue until a V or F-cycle of multigrid iterations is finished. We use a fixed number of smoothing steps of a special 'Vanka' smoother which acts locally in each element Ω_i on all levels and which can be written as:

$$\begin{pmatrix} u^{k+1} \\ v^{k+1} \\ \Theta^{k+1} \\ p^{k+1} \end{pmatrix} = \begin{pmatrix} u^k \\ v^k \\ \Theta^k \\ p^k \end{pmatrix} - \omega^k \sum_{\Omega_i} \begin{pmatrix} S_{uu}|_{\Omega_i} & S_{uv}|_{\Omega_i} & j_1 M|_{\Omega_i} & B_u|_{\Omega_i} \\ S_{vu}|_{\Omega_i} & S_{vv}|_{\Omega_i} & j_2 M|_{\Omega_i} & B_v|_{\Omega_i} \\ S_{\Theta u}|_{\Omega_i} & S_{\Theta v}|_{\Omega_i} & S_\Theta|_{\Omega_i} & 0 \\ B_u^T|_{\Omega_i} & B_v^T|_{\Omega_i} & 0 & 0 \end{pmatrix}^{-1} R \tag{17}$$

with $\mathbf{R} = \left(\text{def}_u^k \ \text{def}_v^k \ \text{def}_\Theta^k \ \text{def}_p^k\right)^T$ (see [14, 17] for more details).

This iteration represents the linearization of equation (14) where the additional nonzero blocks inside the Jacobian arise from the dependency on the vector of unknowns of the nonzero blocks in equation (14). For example, in the temperature row of the matrix in equation (14), the S operator depends on the velocity vector. Hence, there will be nonzero block in the velocity column of the temperature row of the Jacobian. In this way, one can see which block will be nonzero in the local system. The inverse of the local systems on each element Ω_i (of size 30×30) is computed by a direct linear solver.

4 Numerical Analysis

In this section we will present numerical results of benchmarking type for several problems. The first is the MIT Benchmark 2001 [3] where we show that our non-isothermal code can reproduce the benchmark results. Then, we perform numerical simulations for a problem with temperature dependent viscosity. Finally, we add a dissipation term into the energy equation in order to have the effect of viscous heating along the fluid flow and perform corresponding numerical simulations.

4.1 MIT Benchmark 2001

The MIT Benchmark 2001 [3] describes heat driven cavity flow in a 8:1 rectangular domain at near-critical Rayleigh number. Why near-critical? Because the onset of thermal convection will occur at the critical number, beyond that non-periodical up to turbulent flow will occur.

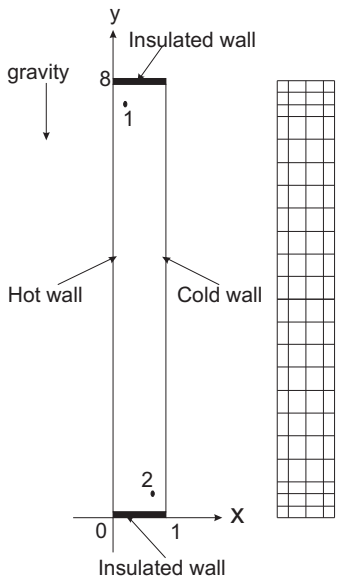

Fig. 2. *Geometry and coarse mesh*

4.1.1 Problem description

The geometry of the problem is very simple, (see Fig. 2). The velocity vector at the upper and bottom wall is zero, which describes a non-slip condition. The left wall is heated while the right wall is cooled by a prescribed non-dimensional temperature of -0.5 and 0.5. Gravity is applied downwards. The top and bottom of the walls are insulated, which means that homogeneous Neumann

boundary conditions for the temperature are set and hence no heat is going outside of the wall. The initial condition is the zero vector for all variables. Physically relevant variables which are to be computed are the velocity and temperature at point 1, and the Nusselt number along the side of the wall. The skewness of the temperature data between point 1 (0.181, 7.37) and 2 (0.819, 0.63) is investigated in time. Since the flow must be skew-symmetric for moderate Rayleigh numbers, the skewness of velocity and temperature between point 1 and 2, as a control of quality, should be close to zero

$$\epsilon_{12}(t) = \Theta_1(t) + \Theta_2(t) = \mathbf{u}_1(t) + \mathbf{u}_2(t) \approx 0. \tag{18}$$

The time step is chosen so that there are enough data points in one oscillation of the resulting variables. After comparison with the results from Turek [13], Davis [6], Gresho [8], and Le Quéré [12] we choose approximately 34 time steps in one oscillation which corresponds to $\Delta T = 0.1$ as time step size.

Table 1
Contributor's meshes and our testing meshes

Author	Turek	Davis	Gresho	Le Quéré
Mesh	90945	83 x 403	105 x 481	48 x 180
Mesh	Elements	Nodes	Edges	Dof
2R	1408	1513	2920	21747
2R_a1	1936	2043	3978	29679
2R_a5	17776	17891	35666	267327
3R	5632	5841	11472	85731
3R_a1	6688	6899	13586	101583
3R_a4	21472	21689	43160	323379
4R	22528	22945	45472	340419
4R_a1	24640	25059	49698	372111
4R_a3	37312	37735	75046	562215

Several meshes are used to perform the spatial discretization, (see Tab. 1). The coarse mesh has approximately 1:5 x-to-y ratio of grid points and decreases gradually to the walls, (see Fig. 3). This figure also describes how the local refinement is generated for some exemplary meshes. The level 2 mesh (2R, meaning 2 times regular refinement of the coarse mesh) is used to perform the first computation until the solution reaches a periodical result (after 1500 non-dimensional time units), then the last output result is used as a starting point for the following computation. Note that regular refinement doubles the number of elements in both x and y direction. Later on, also local refinement along the side of both walls is performed to get a better result for the Nusselt number,

$$Nu(t) = \frac{1}{H} \int_0^H |\frac{\partial \Theta}{\partial x}|_{x=0,W} \, dx \tag{19}$$

where H and W are the height and the width of the domain. The meshes are denoted by nR_ai for i local refinement steps after n regular refinements.

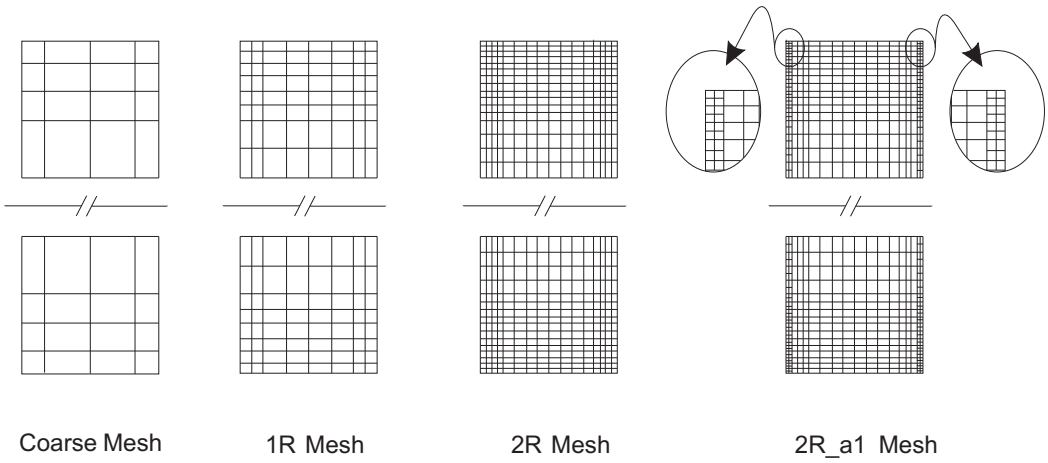

Fig. 3. *Several hierarchies and types of meshes*

4.1.2 Unsteady results of the MIT Benchmark 2001

The results of the MIT Benchmark 2001 configuration computed by our new approach oscillate periodically in time and are presented in Table 2 and 3. Some comparisons are made to see the difference from the other references. In

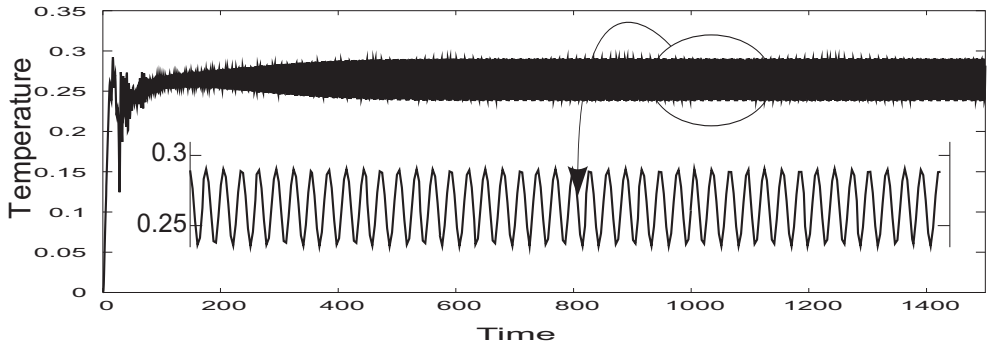

Fig. 4. *Temperature oscillations at point 1*

[8] it is mentioned that the Q_2P_1 element with coarse mesh (27 x 121) performs poorly in the sense that the results show too low amplitudes for velocity and temperature at point 1 (0.00542 and 0.00442). In contrast, we observe good results even with the level 2 mesh (16 x 88). They also calculated Nusselt numbers which are slightly different from the reference, see Le Quéré [12]. In fact, we produce the same results (2R, 3R, 4R), but as soon as we introduce local refinement near the wall, the Nusselt number improves strongly even with the level 2 mesh. It is obvious that the Nusselt number calculated on level 3 and 4 (3R and 4R) can be improved by using the level 2 mesh with local refinement (2R_a1 and 2R_a5). We believe that without local grid refinement we might have to use level 5 or higher to produce nearly the same Nusselt numbers as the one produced by Le Quéré. This information tells us that local grid refinement helps a lot for this test configuration. The time step is not an issue as long as we put enough time steps over one period. 20 up

Table 2
Results of the MIT Benchmark 2001 simulations

Author	u_1	Θ_1	-Nu	Period
Turek	0.0572	0.2647	4.5791	3.422
Davis	0.0563	0.2655	4.5796	3.412
Gresho	0.05665	0.26547	4.5825	3.4259
Le Quéré	0.056356	0.26548	4.57946	3.4115
2R	0.058139	0.26539	4.66245	3.4000
2R_a1	0.057674	0.26538	4.59295	3.4214
2R_a5	0.057490	0.26540	4.57941	3.4214
3R	0.056787	0.26548	4.59318	3.4214
3R_a1	0.056665	0.26546	4.58155	3.4214
3R_a4	0.056591	0.26549	4.57967	3.4214
4R	0.056451	0.26549	4.58158	3.4200
4R_a1	0.056394	0.26546	4.57994	3.4154
4R_a3	0.056372	0.26546	4.57969	3.4214

Table 3
Difference from the reference results in percentage (%)

Author	u_1	Θ_1	-Nu	Mean difference of u_1, Θ_1, -Nu
Turek	1.4976	-0.2938	-0.0078	0.5997
Davis	-0.0993	0.0075	0.0030	0.0366
Gresho	0.5216	-0.0037	0.0663	0.1973
Le Quéré	ref.	ref.	ref.	ref.
2R	3.1638	-0.0323	1.8122	1.66947
2R_a1	2.3390	-0.0361	0.2947	0.88999
2R_a5	2.0125	-0.0267	-0.0010	0.68014
3R	0.7652	0.0027	0.2997	0.35591
3R_a1	0.5496	-0.0061	0.0458	0.20053
3R_a4	0.4177	0.0060	0.0046	0.14283
4R	0.1690	0.0042	0.0463	0.07321
4R_a1	0.0673	-0.0059	0.0105	0.02795
4R_a3	0.0290	-0.0038	0.0051	0.01268

to 40 time steps are already sufficient to produce excellent results for this problem, and no specific gain/loss in the quality of the Nusselt number has been observed if we increase/decrease the number of time steps in one period. Summarizing, we observe differences from the reference result with 0.02% for velocity u_1 and with 0.003% for temperature Θ_1; and we are very close with 0.004% difference for the Nusselt number.

As a conclusion, the new approach produces much better results than the old FeatFlow results [13] using much less degrees of freedoms for the same numerical problems so that we can proceed with more complex non-isothermal problems which we present in the next section.

4.2 Temperature Dependent Viscosity in a Heat Exchanger

Flow with high viscosity through small pipes is very common in heat exchangers which typically leads to a complex flow behavior. In order to study this behavior, a prototypical flow configuration is set in which different temperature values as Dirichlet boundary data at each of the pipes are implemented. Qualitatively, it is expected that the flow will stop when the viscosity grows to a large value caused by temperature differences. Therefore, for prototypical test simulations the viscosity is prescribed through the relation

$$\eta = \eta_0 \; e^{\left(a_1 + \frac{a_2}{a_3 + \Theta}\right)} \; (b_1 + b_2 \; \|\mathbf{D}\|)^{-b_3} \tag{20}$$

where $a_1, a_2, a_3,$ and b_1, b_2, b_3 are specific material parameters, and $\|\mathbf{D}\| = \sqrt{D_{ij} \; D_{ij}}$. Here, $\mathbf{D} = \frac{1}{2}(\nabla \mathbf{u} + \nabla \mathbf{u}^T)$ is the usual symmetric part of the gradi-

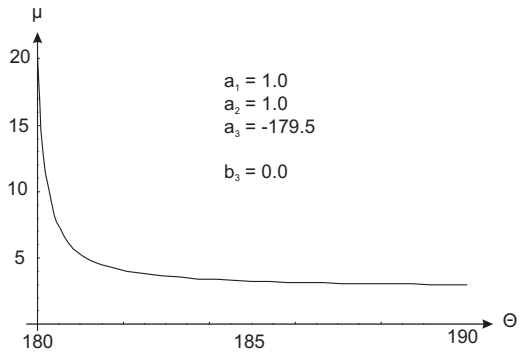

Fig. 5. *Non-dimensional temperature dependent viscosity*

ent velocity. Figure 5 gives an example for specific material parameters which however does not correspond to a certain type of fluid, because we do not yet investigate experimental data for this purpose. Further example with more general parameter settings are examined in [5]. We consider the specific ge-

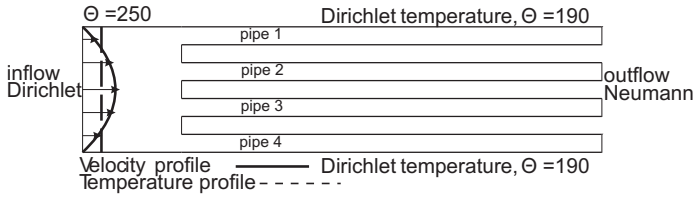

Fig. 6. *Set up for the pipe problem*

ometry (width = 3.5 and length = 44 in non-dimensional units) and setting given in Figure 6 which shows 4 pipes installed for low Reynold number flow ($Re \approx 5$). The hot fluid enters the inflow section with non-dimensional temperature $\Theta = 250$ and with a parabolic profile of velocity, and the heat is then distributed to all pipes. We specify Dirichlet data for the temperature ($\Theta = 190$) to all pipes except to the second pipe ($\Theta = 180$) to control the

fluid flow at this pipe. This slightly different temperature will nevertheless increase the viscosity difference to 'stop' the flow at the corresponding pipe. We present in Figure 7 (euclidean norm of velocity) the resulting flow which almost stops at the second pipe caused by a locally growing viscosity. In the left figure, we start with prescribing the same temperature ($\Theta = 190$) to all pipes (the viscosity value is 0.0029 at all pipes) while in the right figure, we change the temperature at the second pipe to $\Theta = 180$. Hence, viscosity at this pipe grows to 0.0144 (≈ 5 times bigger than before), and finally the flow is stopped at this pipe.

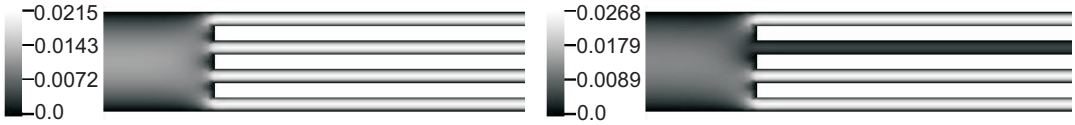

Fig. 7. *Left: The flow is not blocked. Right: The flow at the second pipe is blocked*

Table 4 shows how the proposed method converges with respect to a given number of digits for the linear multigrid solver. Here, #NL denotes the number of Newton iteration, while #MG presents the averaged number of multigrid iterations per nonlinear step. The memory requirement of our computer is still capable to run direct linear solver (UMFPACK) for this problem at least up to 3 refinements. In our case, we can force multigrid by decreasing the number of linear tolerance to get close with UMFPACK results with respect to the number of nonlinear iterations. It is clear that for Tol $= 10^{-8}$ the computation needs more or less the same nonlinear iterations as the ones produced with UMFPACK. In this configuration, we use 8 smoothing steps and all initial solutions start from zero.

Table 4
#NL/#MG for different levels, with Tol denoting the linear stopping criterion

Tol/Level	1R	2R	3R
10^{-1}	10/1	10/2	12/3
10^{-2}	7/2	8/3	8/5
10^{-3}	6/2	6/4	6/7
10^{-8}	5/7	5/11	5/18
UMFPACK	5/-	5/-	4/-

We also test a more complex geometry which is being used in chemical micro-reactor processes, (see Fig. 8). Inside this geometry, we implement the same boundary conditions as for the previous geometry but a different temperature is set for the pipes which lay in the middle of the geometry. Fluid flow is then stopped through these pipes (dark color), and as a result the fluid flows only through the top and bottom pipe of the geometry (grey/white color). The

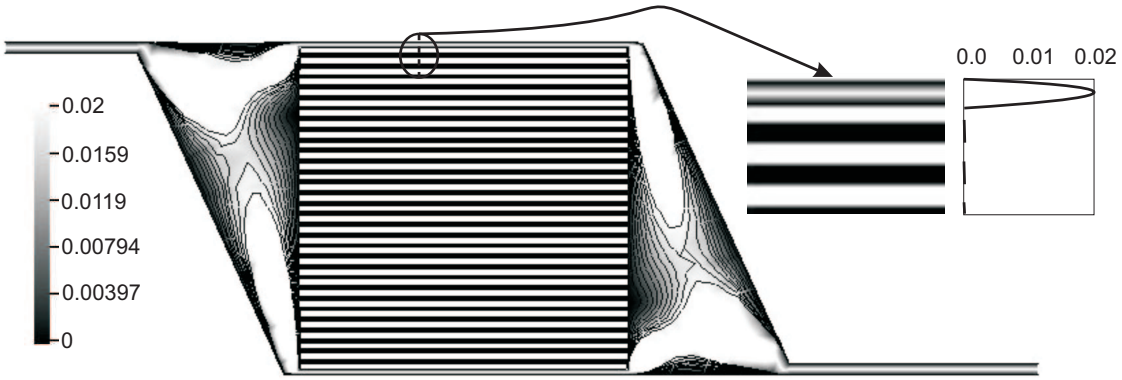

Fig. 8. *The norm of velocity for the stopping flow of the middle pipes*

velocity profile at the cut-line is parabolic for the upper pipe and no flow for the middle pipes. The last example does not only convince us that we can control the fluid flux only by changing slightly the final temperature of the pipes, but also gives us an idea of a "non-mechanical valve" which can be controlled by setting the outside temperature only. One may think of hot pattex material (for glue purpose) which can flow when the temperature increases and which will become an elastic solid when the temperature decreases. Of course, different types of fluid should then be extensively investigated for this purpose.

4.3 Viscous Dissipation Term inside the Energy Equation

Finally, we add a viscous dissipation term into the equation of energy where at the moment the stress tensor is just the symmetric part of the gradient velocity, $\mathbf{T} \equiv \mathbf{D}$ (see [11]). The additional term has the physical meaning of producing viscous heat along with the fluid flow. The heat generated from this friction may dramatically change the temperature and velocity profile of the flow which is of interest in the study of polymer flow. Hence, the new equation can be rewritten as

$$\frac{\partial \Theta}{\partial t} + (\mathbf{u} \cdot \nabla)\Theta = \mathbf{D} : \mathbf{D} + \nabla \cdot (k \nabla \Theta). \tag{21}$$

The new equation is comparable with equation (3) where $k \equiv 1/\sqrt{Ra\ Pr}$ but with an additional term which is defined by a scalar product of the symmetric part of the gradient velocity with itself. We test the modified model with constant viscosity ($\eta = \eta_0$) for the well-known 4 to 1 contraction geometry, (see Fig. 9) and apply a non-slip condition at the upper wall while prescribing the half of the parabolic velocity profile at the inflow due to its symmetry. By neglecting the time derivative ($\frac{\partial \Theta}{\partial t} = 0$), we provide a steady state simulation for this configuration in the sense that time goes to infinity.

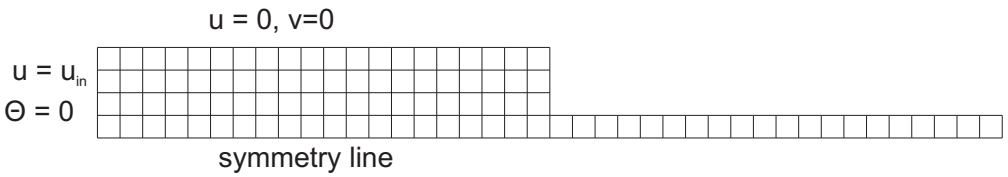

Fig. 9. *Geometry of the 4 to 1 contraction configuration*

Although we prescribe zero temperature at the inflow, along the channel heat is produced as the friction becomes higher. Generally, it gives additional heat locally as the material begins to flow. We refer to Figure 10 to see qualitatively the effect of the additional term. One can see from the cut-line diagram ($y = 0.5$) that near the inflow ($-20 < x < 0$) heat is produced slowly, but that after entering the contraction ($0 < x < 20$) there is a big gradient of temperature up to the end of the channel.

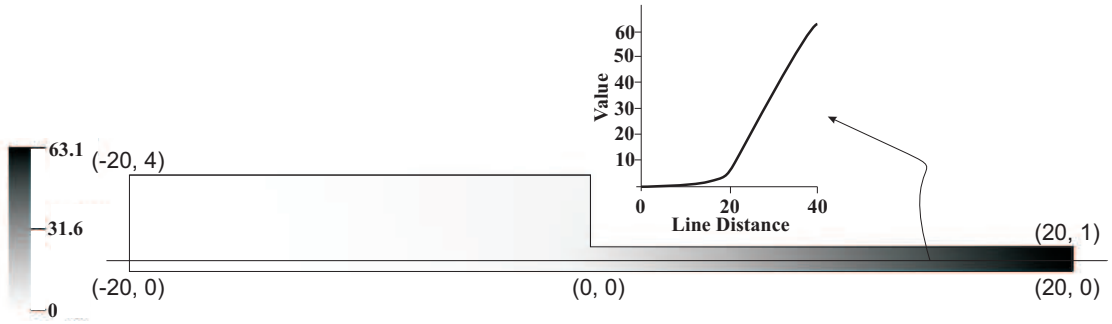

Fig. 10. *The increasing temperature due to friction along the line* $y = 0.5$

These prototypical studies are in preparatory for more complex configurations for which we will extend $\mathbf{T}$ with an additional elastic part of a viscoelastic stress tensor $\boldsymbol{\sigma}^p$ which will replace $\mathbf{D}$ to produce a better physical meaning of additional heat along the flow due to friction (see [5]).

5 Conclusion

We presented new FEM simulation techniques for non-isothermal viscous flow described by the Navier-Stokes equations and the Boussinesq approximation. The resulting discrete problem is solved via discrete Newton iteration and hierarchical multigrid methods utilizing the high order Q_2P_1 FEM pair. Numerical results are provided for the MIT Benchmark 2001 which are non-steady and periodically oscillating for a critical Rayleigh number which makes the post-processing a little bit subjective due to graphical calculation. Nevertheless, our result is comparable if not superior for $Ra = 3.4\ 10^5$. Local refinement plays an important role in giving a better result of the Nusselt number. On the other hand, it does not disturb the non-/linear convergence rates. Additionally, we

simulate two problems with temperature dependent viscosity which may lead to the idea of a non-mechanical valve and with dissipation term inside the energy equation which will be a first step towards viscoelastic flow. Preliminary results are shown to see qualitatively the behavior of the flow as motivation for further research purpose.

6 Reference

[1] Arnold, D. N., Boffi, D., and Falk, R. S. *Approximation by Quadrilateral Finite Element*, Math. Comput., 71(239):909-922, 2002.

[2] Boffi, D. and Gastaldi, L. *On the Quadrilateral Q2-P1 Element for the Stokes Problem*, Int. J. Numer. Meth. Fluids, 39:1001-1011, 2002.

[3] Christon, M. A., Gresho, P. M., Sutton, S. B. *Computational predictability of natural convection flows in enclosures*. In: Computational Fluid and Solid Mechanics, 40:1465-1468, First MIT Conference on Computational Fluid and Solid Mechanics, Elsevier, 2001.

[4] Christon, M. A., Gresho, P. M., Sutton, S. B. *Computational predictability of natural convection flows in enclosures*. International Journal for Numerical Methods in Fluids, 40:953-980, 2002.

[5] Damanik, H., Hron, J., Ouazzi, A., Turek, S. *A monolithic FEM approach for temperature and shear dependent viscosity in viscoelastic flow*. To appear in 2008.

[6] Davis, D., Bänsch, E. *An operator-splitting finite-element approach to the 8:1 thermal cavity problem*. International Journal for Numerical Methods in Fluids, 40:1019-1030, 2002.

[7] Gresho, P. M. *On the theory of semi-implicit projection methods for viscous incompressible flow and its implementation via a finite element method that also introduces a nearly consistent mass matrix, part 1: Theory*, Int. J. Numer. Meth. Fluids, 11: 587-620, 1990.

[8] Gresho, P. M., Sutton, S. B. *Application of the FIDAP code to the 8:1 thermal cavity problem*. International Journal for Numerical Methods in Fluids, 40:1083-1092, 2002.

[9] Hron, J., Turek, S. *A monolithic FEM/Multigrid Solver for ALE formulation of fluid structure interaction with application in biomechanics*, Bungartz, H.-J.; Schfer, M., Lecture Notes in Computational Science and Engineering, 53, 146-170, Fluid-Structure Interaction - Modelling, Simulation, Optimization, Springer, ISBN 3-540-34595-7, 2006.

[10] Rannacher, R. and Turek, S. *A Simple nonconforming quadrilateral Stokes element*, Numer. Methods Partial Differential Equations, 8:97-111, 1992.

[11] Schowalter, W. R. *Mechanics of Non-Newtonian Fluids*, Pergamon Press, 1978.

[12] Shihe Xin, Le Quéré, P. *An extended Chebyshev pseudo-spectral benchmark*

for the 8:1 differentially heated cavity. International Journal for Numerical Methods in Fluids, 40:981-998, 2002.

[13] Turek, S., Schmachtel, R. *Fully coupled and operator-splitting approaches for natural convection flows in enclosures*. International Journal for Numerical Methods in Fluids, 40:1109-1119, 2002.

[14] Turek, S. *Efficient Solvers for Incompressible Flow Problems: An Algorithmic and Computational Approach*, LNCSE 6, Springer-Verlag, 1999.

[15] Turek, S., Rivkind, L., Hron, J., Glowinski, R. *Numerical Study of a Modified Time-Steeping theta-scheme for incompressible flow simulations*, Journal of Scientific Computing, 28, 2-3, 533-547, http://dx.doi.org/10. 1007/s10915-006-9083-y, 2006.

[16] Turek, S., Hron, J. *A monolithic FEM solver for an ALE formulation of fluid-structure interaction with configuration for numerical benchmarking*, Wesseling, P., Onate, E., Periaux, J., 176, Books of Abstracts European Conference on Computational Fluid Dynamics, Eccomas CFD 2006, 2006.

[17] Turek, S., Ouazzi, A., Hron, J. *A Computational Comparison of two FEM Solvers For Nonlinear Incompressible Flow*, Bänsch, E., LNCSE, 87-109, Challenges in Scientific Computing CISC 2002, Springer, ISBN 3-540-40887-8, 2002.

[18] Wesseling, P. *An Introduction to Multigrid Methods*, John Wiley & Sons, 1992.

[19] Yanhu Guo, Bathe, K. J.*A numerical study of a natural convection flow in a cavity*. International Journal for Numerical Methods in Fluids, 40:1045-1057, 2002.